2025 IEEE/SICE International Symposium on System Integration (SII)
January 21-24, 2025, Munich, Germany

Empirical Strength Comparison of 3D printed Beams and Proposal of a Joining Method for Large Parts*

Norisato Kanai[1], Hiroyuki Nabae[1], and Gen Endo[1]

Abstract— **Several challenges arise when considering the application of 3D-printed parts to robotics. First, there is less discussion on bending strength. Second, variations in bending strength occur depending on the type of 3D printer used. Third, the fabrication of large-scale parts remains difficult. In this study, to address the first challenge, we conducted three-point bending tests on specimens with dimensions deviating from standardized specifications, revealing discrepancies in material properties and emphasizing the importance of filament crystallization. For the second challenge, we fabricated identical test specimens under the same conditions using two different 3D printers. We performed three-point bending tests, thereby elucidating the variability in bending strength attributable to the printer type. To address the third challenge, we proposed a joining method involving the mating and adhesion of square-pyramidal convex/concave parts and demonstrated its effectiveness through three-point bending tests.**

I. Introduction

In recent years, the increasing usage of 3D printers has been remarkable[1][2][3]. Various types of 3D printing technologies exist, including fused filament fabrication (FFF), stereolithography (SLA), material jetting, and binder jetting, which deal with resin materials[4]. Metal-based technologies include selective laser melting (SLM), among others[5][6]. FFF, in particular, involves the extrusion of thermoplastic filament material heated to its melting point. It is currently the most widely used method due to its ease of filament purchasing and low cost.

One of the significant advantages of 3D printing technology is its ability to create complex shapes that are challenging to achieve using traditional manufacturing methods. Additionally, 3D printing imposes fewer restrictions on material usage, making it appealing across various fields, such as food, automotive, and aerospace industries[6]. In industrial robotics, replacing traditional structural parts with 3D printed parts has the potential to reduce weight, lower costs, and enhance performance. However, several challenges exist when applying 3D printing technology to robotic applications, which are outlined below:

1) **Less Discussion on Strength:** Currently, discussions on material strength are primarily based on standardized test specimens. Although 3D printing technology offers high design flexibility, the material strength in complex geometries is often uncertain. Manufacturers typically provide strength and stiffness data based on ISO or JIS standard test specimens, but the applicability of this data to actual parts is unclear. Therefore, it is crucial to conduct strength tests on parts with shapes and sizes that differ from standard test specimens.
2) **Variations in Strength across Printers:** Even when fabricating the same object, significant differences in strength can arise due to factors such as extrusion speed, head movement speed, and nozzle shape[7][8].
3) **Difficulties in Fabricating Large Parts:** Fabricating large parts, such as robot arms, using 3D printing is challenging due to the limitations of print volume. Although using larger 3D printers can increase build size[9][10], such machines are often complex, expensive, and require significant installation space. While belt-type 3D printers[11] have been proposed as an alternative, they are limited by height restrictions and lower versatility. Moreover, large-scale fabrication increases the difficulty of preventing warping caused by thermal shrinkage and maintaining high precision[12]. To address these challenges, a novel joining method that maintains bending strength while assembling smaller parts into larger ones is needed. Past studies have proposed methods inspired by traditional woodworking joints, but these approaches have shown up to a 75% reduction in strength compared to nominal filament strength[13]. This study proposes a new joining method optimized for 3D printed parts and evaluates its effectiveness through bending tests.

Based on this background, the objectives of this study are as follows:

- To verify whether the strength provided by manufacturers can be achieved in parts with dimensions that differ from standard test specimens.
- To investigate the variation in strength when the same object is fabricated using different 3D printers under identical conditions.
- To propose a novel joining method for 3D printed parts and experimentally evaluate its bending strength.

II. Verification of Bending Strength for Specimens Differing from Standard Specifications

In this section, we conducted tests on three types of specimens with dimensions differing from the standard test specimen specified by the regulations, under two conditions: with and without annealing. For each condition, we calculated the bending modulus and bending strength.

*This research is subsidized by New Energy and Industrial Technology Development Organization (NEDO) under a project JPNP20016.

[1]Norisato Kanai, Hiroyuki Nabae, and Gen Endo are with the Department of Mechanical Engineering, Institute of Science Tokyo, 2-12-1 Ookayama, Meguro-ku, Tokyo 152-0033, Japan kanai.n.ab@m.titech.ac.jp

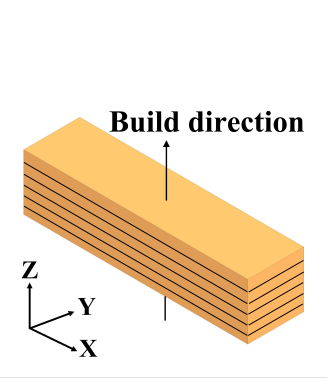

Fig. 1. Direction X-Y

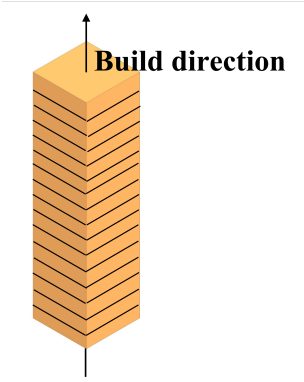

Fig. 2. Direction Z-X

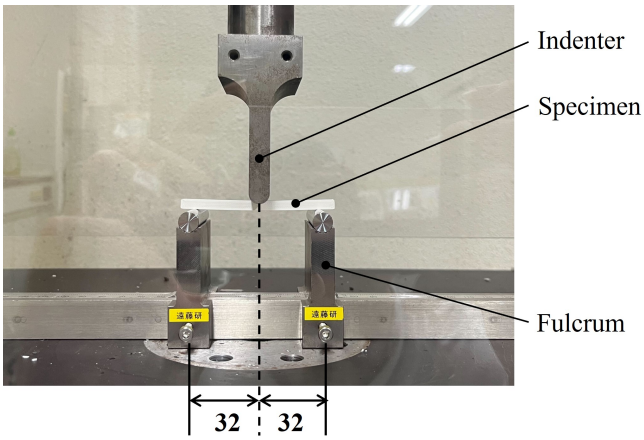

Fig. 3. Three-point bending test

A. Test Conditions

The material used in this study is a potassium titanate fiber-reinforced filament (POTICON filament NTL34M, Otsuka Chemical Co., Ltd.). NTL34M, which consists of 20w% potassium titanate in a bio-based PA (nylon), is recognized for its exceptional impact and wave resistance. Among non-carbon continuous fiber filaments for standard FFF 3D printers, POTICON NTL34M is one of the strongest materials, with applications in cycloidal reducers[14] and quadruped robots (TITAN-E1[15]), and is anticipated for broader future uses. The physical properties of POTICON are shown in Table I.

Three-point bending tests were conducted using specimens with dimensions of $5 \times 5 \times 80\,\mathrm{mm}, 5 \times 5 \times 160\,\mathrm{mm}, 5 \times 5 \times 240\,\mathrm{mm}$ to test different path length for one layer. They are fabricated in the X-Y direction. In this paper, the term X-Y direction refers to specimens fabricated horizontally (Fig. 1), while Z-X direction refers to specimens fabricated vertically (Fig. 2). The arrows in Fig. 1 and 2 indicate the layering direction.

3D printed objects consist of layers bonded by melted filament fusion. However, unlike homogeneous materials, layer interfaces weaken the overall strength. In FFF, parts fabricated in the X-Y direction generally exhibit higher bending strength in the three-point bending test (Fig. 3) compared to those fabricated in the Z-X direction.

In this study, we first perform fabricating with standard settings, assuming a typical user, and conduct three-point bending tests to demonstrate the deviation from the manufacturer's provided values. Next, based on previous experience and advice from material manufacturers, we improve the fabricating parameters and testing environment. Subsequently, we compare the bending strength with and without annealing (and the associated crystallization of the filament) to highlight the importance of crystallization.

TABLE I

PHYSICAL PROPERTIES OF POTICON FILAMENT NTL34M

Physical properties	Physicasl property value	
Glass transition temperature [°C]	60	
Density [g/cm^3]	1.27	
Laminating direction	X-Y	Z-X
Tensile strength [MPa]	114	68
Tensile elongation [%]	4.1	4.8
Tensile modulus [GPa]	5.6	2.7
Bending strength [MPa]	199	107
Bending modulus [GPa]	7.0	2.8

TABLE II

STANDARD SETTINGS

Parameters	Value
3D printer	G-ZERO
Slicer software	Prusa Slicer
Nozzle diameter [mm]	0.4
Pitch [mm]	0.1
Number of shells	3
Extrusion width [mm]	0.42
Fill density [%] / Pattern	100 / Straight (45°)
Nozzle temperature [°C]	270
Platform temperature [°C]	50

The 3D printer used in this study was G-ZERO (Gutenberg Co., Ltd), and the slicing software employed was PrusaSlicer (PRUSA RESEARCH a.s.).

The three-point bending test was conducted using the Autograph (Shimadzu Corporation: AGX-20kNVD), adhering to JIS K7171 standards. The span was set at 64 mm, with a test speed of 2 mm/min and an indenter radius of 5 mm. Strain and bending stress were recorded until fracture occurred, with the setup illustrated in Fig. 3.

B. Test Results

First, we verify the bending strength obtained when fabricating with standard settings, assuming a typical user. The fabricating parameters are provided in Table II

Here, the infill pattern of straight lines at 45° is depicted as shown in Fig. 4.

The test results under these conditions are shown in Fig. 5 and Table III (the values in parentheses in Table III are the manufacturer's provided values).

As a result, the bending modulus was slightly above 70% of the provided value, and the bending strength was slightly above 50% of the provided value. In other words, when fabricating with the default slicer settings, only about

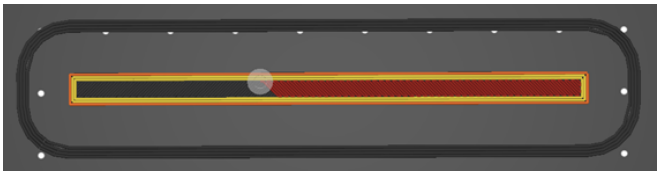

Fig. 4. Infill pattern (Linear 45°)

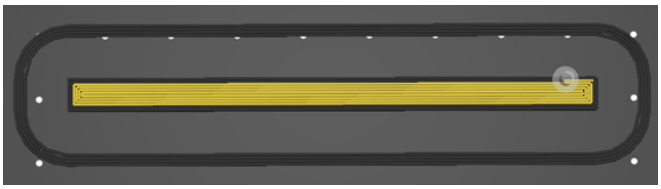

Fig. 6. Infill pattern (Concentric)

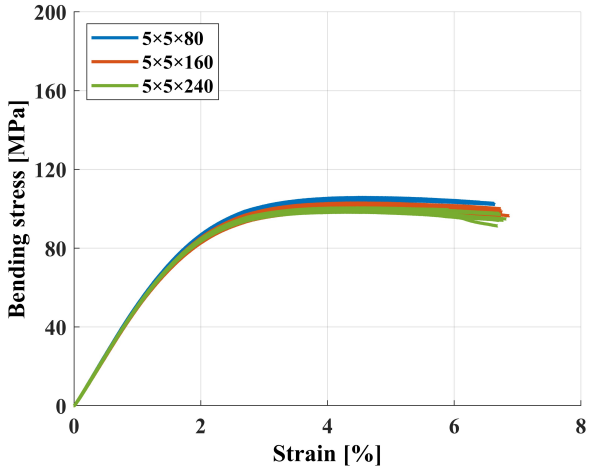

Fig. 5. Results of the three-point bending test (Standard settings)

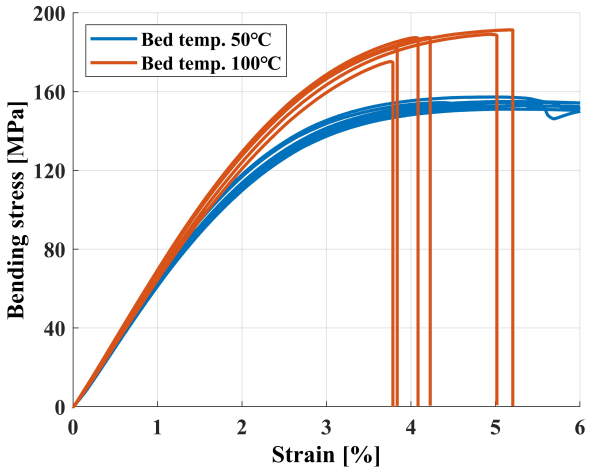

Fig. 7. Bending stress-strain diagram for variations in bed temperature

half of the expected strength is achieved. Furthermore, a slight decrease in bending strength was observed as the path length increased. However, the more critical observation is that the bending strength was significantly lower than the manufacturer ' s provided value. This result could pose significant issues in design. Next, based on previous experience and advice from material manufacturers, the fabricating parameters and testing environment were improved as shown in Table IV.

The detailed explanations are omitted, but these improvements are intended to increase the bending strength of the test specimens and maintain a dry condition. The path of the print after the improvements is shown in Fig. 6. Assuming that the most significant factor affecting bending strength in Table IV is the element ②, we changed only the bed temperature of ②, while keeping the other conditions constant, and performed the three-point bending test. The test specimens for this experiment were sized at $5 \times 5 \times 80$ mm. The results are shown in Fig. 7 and Table V.

As a result, by appropriately setting the fabricating parameters and testing environment, the bending modulus was improved to 94.2% of the provided value, and the bending strength was increased to 93.2% of the provided value. Additionally, it was found that when the bed temperature was lower, the bending modulus decreased by 4.54%, and the bending strength decreased by 16.8% compared to when the bed temperature was higher.

TABLE III

RESULT OF THREE-POINT BENDING TEST (STANDARD SETTINGS)

	Bending modulus [GPa] (7.0)	Bending strength [MPa] (199)
$5 \times 5 \times 80$	5.203	105.0
$5 \times 5 \times 160$	5.069	101.3
$5 \times 5 \times 240$	5.139	99.45

TABLE IV

MODIFIED CONDITIONS / PARAMETERS

	Before	After
① Drying time before use	60°C / 3 days	75°C / 3 days
② Bed temperature	50°C	100°C
③ Infill pattern	Straight (45°)	Concentric
④ Shell number	3	40 (all shell)
⑤ Storage method	Polyethylene pouch	Aluminum pouch
⑥ Desiccant	Silica gel	OZO-Z[16]

C. Discussion

- When fabricating with settings assumed for a standard user, only about 50% of the provided bending strength is achieved.
- By using the settings shown in Table IV, it is possible to achieve a bending modulus of 94% and a bending

TABLE V

SUMMARY OF RESULTS (BED TEMPERATURE AND BENDING STRENGTH)

	Bending modulus [GPa] (7.0)	Bending strength [MPa] (199)
Bed temp. 50°C	6.293	154.3
Bed temp. 100°C	6.592	185.5

strength of approximately 93% of the provided values.

- It is believed that when fabricating at a higher bed temperature, an effect similar to annealing occurs during the fabricating process, resulting in the crystallization of the filament in the test specimens and consequently improving the bending strength. Annealing causes the molecular chains to align in a regular pattern, forming a crystalline structure. The increase in this crystalline structure strengthens the intermolecular interactions, enhancing the overall rigidity and strength of the material. When fabricating at a lower bed temperature, crystallization does not progress, leading to a reduction in bending strength by several tens of percent compared to the provided values. Since the test specimens in this experiment were small, annealing progressed during the fabricating process when the bed temperature was raised. However, for larger parts, crystallization during fabrication is unlikely to occur (The manufacturer recommends post-fabrication heat treatment at 120 °C for 2 hours to promote crystallization).
- The values obtained in this study are the results of fabricating and testing under the best possible conditions. It is important to note that small changes in the fabricating parameters or environment can significantly affect the strength. For example, when used in components such as robots, there is a high likelihood that moisture absorption will occur over time, potentially altering the material properties. In conclusion, relying entirely on the provided values for aggressive design carries risks, and it is crucial to conduct design with sufficient strength margins to ensure reliability.

III. Comparison of Bending Strength Using Different 3D Printers

In this section, we conducted a strength comparison by performing three-point bending tests on specimens fabricated with two different 3D printers under identical conditions, excluding the fabricating speed[1].

A. Test Conditions

The 3D printers used for comparison were G-ZERO and RAISE3D Pro2 (RAISE 3D Technologies, Inc.). Both printers utilized the slicing software IdeaMaker (RAISE 3D technologies, Inc.), and the material used was POTICON, as described in Section II. The dimensions of the specimens were set to $20 \times 20 \times 80\,\mathrm{mm}$, following the subsequent research in the next section, and the fabricating direction was set to X-Y. The fabricating parameters and testing environment are the same as Table IV.

Other than the detailed settings listed in Table IV, the slicer software settings of both printers were unified. The only variable was the fabricating speed. For fabricating speed, the standard values for each printer were used: $200\,\mathrm{mm/s}$ for G-ZERO and $60\,\mathrm{mm/s}$ for RAISE3D Pro2. The total fabricating times were 2h21min for G-ZERO and 4h29min for RAISE3D Pro2, with the mass of the fabricated specimens being $41.0\,\mathrm{g}$ for both.

The test method, as in Section II, involved a three-point bending test using the Autograph (Shimadzu Co., AGX-20kNVD). Six specimens were fabricated for each condition, and the tests were conducted accordingly. It should be noted that for thick components such as these, the method for calculating bending modulus specified in the JIS standard is not suitable. Therefore, the bending modulus was not calculated in this study.

[1]Ideally, all printers should be compared under identical fabrication conditions to ensure fairness. However, in most cases, different slicer software is required for each printer, making it practically impossible to perfectly standardize the conditions. Therefore, this study conducted a comparison using two printer models that can utilize the same slicer software.

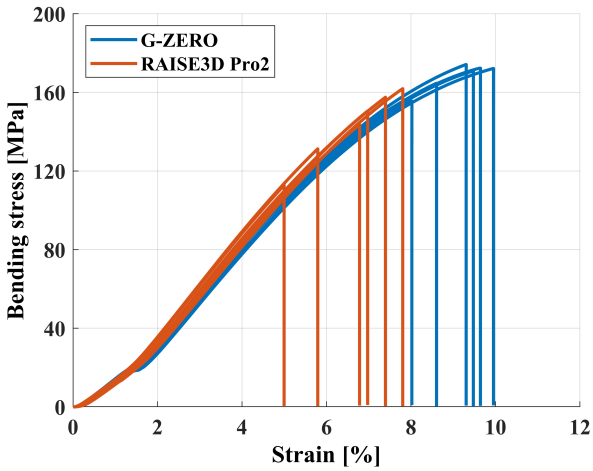

Fig. 8. Bending stress-strain diagram for each 3D printer

TABLE VI
Summary of Results (A Comparison of Two 3D Printers)

3D printer	Bending strength [MPa]		Unbiased variance [MPa^2]
G-ZERO	Max	174.2	49.91
	Min	155.5	
	Average	168.3	
RAISE3D Pro2	Max	161.9	335.7
	Min	112.7	
	Average	142.9	

B. Test Results

The test results are shown in Fig. 8 and Table VI. The values in Table VI represent the average of the test results. G-ZERO exhibited higher values for bending strength compared to RAISE 3D Pro2.

C. Discussion

- Compared to the specimens fabricated using RAISE3D Pro2, those fabricated with G-ZERO exhibited 17.8% higher bending strength. Since the only difference in the fabrication conditions between the two 3D printers was the fabricating speed, it is possible that in the case of G-ZERO, the previous layer retained more heat, allowing for better interlayer bonding and increased strength.

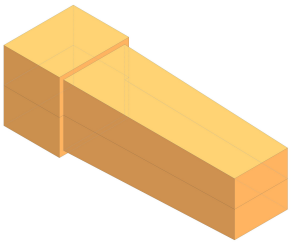

Fig. 9. Convex part

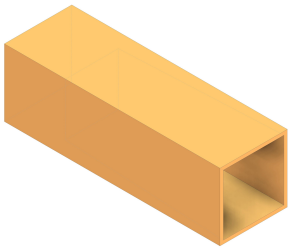

Fig. 10. Concave part

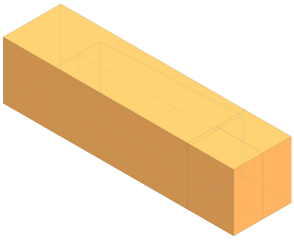

Fig. 11. After joining

Fig. 12. Parallel cracks

Fig. 13. Vertical cracks

However, this cannot be conclusively determined at this stage.

- Among the 12 test specimens, the difference between the lowest and highest bending strength was approximately 60 MPa. Additionally, RAISE 3D Pro2 exhibited greater variability in bending strength compared to G-ZERO. While fine-tuning the parameters may reduce this variability and achieve higher strength, it is important to recognize that even if a typical user prints the same test specimens under the same conditions, variations in strength on the order of tens of percent will still occur. This variability must be considered during the design process.

IV. Proposal of Joining Method for Large-Scale Parts

This section first proposes a novel joining method with high strength and versatility and describes the method for determining the shape. The effectiveness of this method is demonstrated through strength evaluation using three-point bending tests. The target shape of the parts are square beams used in applications such as robotic arms, with the load assumed to be bending.

A. Proposed Joining Method

The proposed method involves joining through the mating and bonding of square pyramidal-shaped convex and concave parts. Fig. 9 illustrates the convex part, while Fig. 10 shows the concave part. The dimensions are as follows: width 20 mm, height 20 mm, with the projection's root from the end of the convex part being 16 mm, and the projection root measures 18×18 mm, with a projection length of 48 mm.

In manufacturing, the convex part is divided into two sections relative to the Z-X plane and fabricated in the X-Y direction. After bonding with adhesive, it is mated and bonded to the concave part so that the joining interface is orthogonal to the build table. The concave part, with a length of 64 mm, is fabricated in the Z-X direction. The dimensions of the joined convex and concave parts are $20 \times 20 \times 80$ mm (Fig. 11).

The rationale for this shape is as follows:

- **The joining interface is as perpendicular as possible to the bending load direction:** The direction of the weakest crack under bending is parallel to the load (Fig. 12). Therefore, joining the member vertically along its length is the weakest approach. If the crack direction is perpendicular to the bending load, the force driving crack propagation is not directly applied, and thus, the strength can be maintained (Fig. 13). Ideally, the 3D printing layer interface should be perpendicular to the force direction, but this conflicts with elongating the part. Therefore, a diagonal joining approach was considered optimal.
- **The adhesive is easier to apply:** If the convex part is completely parallel to the concave part's wall, the adhesive tends to peel off during mating. By introducing a taper, the adhesive can be pushed into the bottom of the concave part and distributed more evenly during bonding.
- **Symmetry in all directions:** Since loads from various directions are anticipated, it is desirable for the shape to be independent of direction.
- **Resistance to moments around the long axis:** Although mating with a conical shape meets the three conditions mentioned above, conical shapes are believed to offer less resistance to moments (twisting) around the long axis. A square pyramid shape can provide greater resistance.

The method for determining the protrusion is described here. As an example, consider inserting part B into part A, which is a rectangular prism with width and height of a and a central square hole with length x (Fig. 14). Let the Young's modulus of part A be E_A and that of part B be E_B, with the condition that $E_A < E_B$. The second moment of area of this composite member is calculated by correcting the second moments of area of parts A and B based on their respective Young's moduli. The second moment of area I is given by the following equation:

$$I = I_A + I'_B \tag{1}$$

Here, I_A is the second moment of the area of part A, and I'_B is the equivalent second moment of the area of part B. I'_B

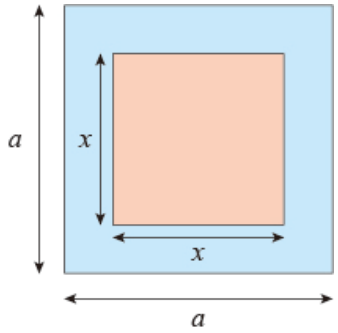

Fig. 14. A bar with a side length of a and a square hole with a side length of x cut out

is transformed using Young's modulus ratio $n = E_B/E_A$ as follows:

$$I_B' = n \cdot I_B \tag{2}$$

Also, if the bending stresses acting on parts A and B are denoted as σ_A and σ_B, respectively, we have the following relations:

$$\sigma_A = \frac{My_A}{I}, \sigma_B = \frac{My_B}{I} \cdot \frac{E_A}{E_B} \tag{3}$$

Where M is the bending moment and y_A and y_B are the distances from the neutral axis of each part. From (3), it is clear that irrespective of the distance from the neutral axis, $\sigma_A > \sigma_B$, and thus, part A will crack first, leaving part B intact, regardless of the width and height of the hole (i.e., the dimensions of part B). If we assume that the hole has a square shape with side length x, the second moment of area I_{quad} is given by:

$$I_{quad} = \left(\frac{a^4}{12} - \frac{x^4}{12}\right) + \frac{E_B}{E_A} \cdot \frac{x^4}{12} = \left(1 - \frac{E_B}{E_A}\right)\frac{x^4}{12} + \frac{a^4}{12} \tag{4}$$

From (4), it can be seen that I depends on x, and as x approaches a, I increases. Hence, the bending strength also increases. Therefore, the shape of part B that maximizes the second moment of area is the optimal one. Applying this concept to the present joining method, part A is the concave part and part B is the convex part, and to maximize the overall bending strength of the part, the design should aim to maximize the second moment of area of the convex part at the point of bending load. In this study, the dimensions were determined such that the length of the side of the convex part at the bending load point is 16.383 mm.

B. Test Conditions

The material used in this study is POTICON, as described in sections II and III. The 3D printer used is G-ZERO, and the slicing software is PrusaSlicer. Comparisons were made among specimens of dimensions $20 \times 20 \times 80$ mm with 100% infill, fabricated in the Z-X direction, and specimens of the same dimensions and infill, fabricated in the X-Y direction (from now on referred to as Specimen (Z-X) and Specimen (X-Y), respectively), as well as the proposed joining method. Three specimens of each Specimen (Z-X) and Specimen (X-Y) were prepared, and six specimens using the proposed joining method were created. Three-point bending tests were conducted.

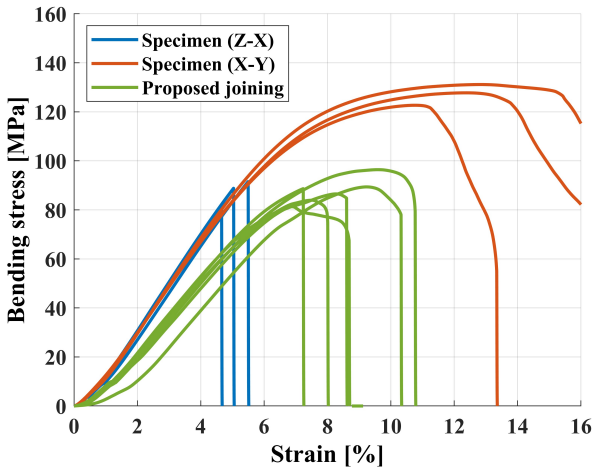

Fig. 15. The bending S-S diagram of the test specimen using the proposed joining method and the test specimen fabricated as a single piece

TABLE VII
SUMMARY OF RESULTS (PROPOSED JOINING METHOD)

Specimen	Bending strength [MPa]
Specimen (Z-X)	87.38
Specimen (X-Y)	127.2
Proposed joining	87.81

C. Test Results

The test results are shown in Fig. 15 and Table VII. The values in Table VII represent the average of the respective test results. When using the proposed joining method, the bending strength was comparable to or greater than that of Specimen (Z-X) and reached approximately 70% of Specimen (X-Y).

D. Discussion

- Using the proposed joining method, bending strengths of 100.5% for Specimen (Z-X) and 69.0% for Specimen (X-Y) were achieved. Although joining introduces an artificial crack, the bending strength being almost equivalent to that of Specimen (Z-X) suggests that the strength reduction due to joining is minimal.
- Based on the results, the proposed joining method demonstrates adequate performance for practical application in parts such as robotic arms.
- In this study, the shape was designed to increase the cross-sectional area at the tip of the convex protrusion, thereby enlarging the bonding surface area parallel to the direction of the bending load. This shape may result in reduced strength under the applied load. Therefore, it is necessary to determine the optimal shape based on the specific load distribution.

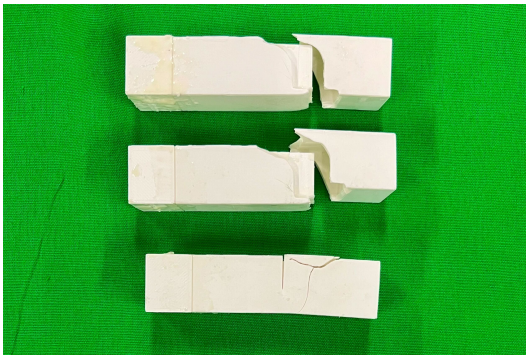

Fig. 16. Test specimens after a three-point bending test using the proposed joining method

V. CONCLUSIONS

This paper addressed three key challenges in 3D printing: 1. Uncertain strength, 2. Strength variability across different printers, and 3. Difficulty in fabricating large-scale parts.

To address Challenge 1, three-point bending tests were conducted on specimens with non-standard dimensions to assess actual bending strength under standardized conditions. As a result, it was confirmed that annealing allows both the bending modulus and bending strength to achieve over 90% of the values listed in the datasheet. Additionally, it was also confirmed that without annealing, both the bending modulus and bending strength significantly decrease.

For Challenge 2, the same object was fabricated using two different 3D printers with identical fabricating parameters, and a strength comparison was conducted using a three-point bending test. As a result, the difference between the maximum and minimum bending strength values of the 12 test specimens was approximately 70 MPa, and some 3D printers exhibited high variability. It is concluded that even when fabricating the same part, it is necessary to account for such strength variations in the design.

In response to Challenge 3, a joining method involving the mating and bonding of square pyramidal convex and concave parts was proposed and validated through three-point bending tests. The method achieved bending strengths of 100.5% for Specimen (Z-X) and 69.0% for Specimen (X-Y). Given the practical strength achieved, this method shows promise for applications in elongated parts such as robotic arms.

We believe that this paper offers valuable insights into the application of 3D printed parts in robotics. In the future, this study's findings will be utilized as a foundation to pursue applications in more practical robotic structural materials.

ACKNOWLEDGEMENT

This research is subsidized by New Energy and Industrial Technology Development Organization (NEDO) under a project JPNP20016. This paper is one of the achievements of joint research with ROBOT Industrial Basic Technology Collaborative Innovation Partnership (ROBOCIP).

We thank Prof. Naoyuki Takesue (Tokyo Metropolitan University), Prof. Yusuke Ota (Chiba Institute of Techonology), and Prof. Takeshi Takaki (Hiroshima University) for their valuable comments and discussion.

REFERENCES

[1] Wan Jiafu, Cai Hu, and Zhou Keliang. Industrie 4.0: enabling technologies. In *Proceedings of 2015 international conference on intelligent computing and internet of things*, pages 135–140. IEEE, 2015.

[2] Siddique Taha Hasan Masood, Sami Iqra, Nisar Malik Zohaib, Naeem Mashal, Karim Abid, and Usman Muhammad. Low cost 3d printing for rapid prototyping and its application. In *2019 Second International Conference on Latest trends in Electrical Engineering and Computing Technologies (INTELLECT)*, pages 1–5. IEEE, 2019.

[3] Sisca Francesco G, Angioletti Cecilia M, Taisch Marco, and Colwill James A. Additive manufacturing as a strategic tool for industrial competition. In *2016 IEEE 2nd International Forum on Research and Technologies for Society and Industry Leveraging a better tomorrow (RTSI)*, pages 1–7. IEEE, 2016.

[4] Shahrubudin Nurhalida, Lee Te Chuan, and Ramlan R.J.P.M. An overview on 3D printing technology: Technological, materials, and applications. *Procedia manufacturing*, 35:1286–1296, 2019.

[5] Calignano Flaviana, Diego Manfredi, Elisa Paola Ambrosio et al. Overview on additive manufacturing technologies. *Proceedings of the IEEE*, 105(4):593–612, 2017.

[6] AHN Jinsung, Murakami Kenichi, HIRANO Masahiro et al. Dynamic compensation system development for advanced 3D printing and its evaluation. *Transactions of the JSME (in Japanese)*, 89, 11 2023.

[7] Márton Tamás Birosz and Dániel Ledenyák and Mátyás Andó. Effect of FDM infill patterns on mechanical properties. *Polymer Testing*, 113:107654, 2022.

[8] Travieso-Rodriguez, J. Antonio and Jerez-Mesa, Ramon and Llumà, Jordi and Traver-Ramos, Oriol and Gomez-Gras, Giovanni and Roa Rovira, Joan Josep. Mechanical Properties of 3D-Printing Polylactic Acid Parts subjected to Bending Stress and Fatigue Testing. *Materials*, 12(23), 2019.

[9] Barnett Eric and Gosselin Clément. Large-scale 3D printing with a cable-suspended robot. *Additive Manufacturing*, 7:27–44, 2015.

[10] Zhang Xu, Li Mingyang, Lim Jian Hui, Weng Yiwei et al. Large-scale 3D printing by a team of mobile robots. *Automation in Construction*, 95:98–106, 2018.

[11] CREALITY. CR-30 FDM 3D printer. Accessed on May 13, 2024.

[12] Bisheh Mohammad Najjartabar, Chang Shing I, and Lei Shuting. A layer-by-layer quality monitoring framework for 3D printing. *Computers & Industrial Engineering*, 157:107314, 2021.

[13] Yuta Tsukamoto, Hiroyuki Nabae, and Gen Endo. Application of Joint Processing in Wood to 3D Printed Parts. *ROBOMECH2023 (in Japanese)*, pages 1A2–I21, 2023.

[14] Akifumi Okubo, Hiroyuki Nabae, Gen Endo. Mechanical Parts Manufactured by a 3D Printer for Industrial Robot -Part5: Durability Test of a Plastic Trochoidal Gear Reducer-. *ROBOMECH2023 (in Japanese)*, pages 1A2–I20, 2023.

[15] Shuhei Tsunoda, Hiroyuki Nabae, Koichi Suzumori and Gen Endo. Development of Quadruped Robot TITAN-E1 Using Plastic Structual Parts Printed by Fused Deposition Modeling. *ROBOMECH2022 (in Japanese)*, pages 2A1–Q07, 2022.

[16] OZO Kagakugiken Co., Ltd. OZO-Z. Accessed on 06.11.2024.